Electronic properties of single-phased metastable Ag-Cu alloys

J. Banhart
Fraunhofer-Institut für Angewandte Materialforschung, Lesumer Heerstrasse 36, 2820 Bremen 77, Federal Republic of Germany

H. Ebert
Siemens AG, ZFE BT MR 11, Paul-Gossen-Strasse 100, 8520 Erlangen, Federal Republic of Germany

R. Kuentzler*
Institut de Physique et Chimie des Materiaux de Strasbourg, 3 rue de l'Université, 67084 Strasbourg, France

J. Voitländer
Institut für Physikalische Chemie, Universität München, Sophienstrasse 11, 8000 München 2, Federal Republic of Germany
(Received 18 May 1992)

We report on results of the measurement of the linear specific-heat coefficient, the magnetic susceptibility, the ^{63}Cu NMR Knight shift, and the ^{63}Cu NMR spin-lattice relaxation time of single-phased metastable Ag-Cu alloys prepared by means of rapid quenching techniques. Difficulties in preparing the metastable alloys are discussed in some detail. Self-consistent Korringa-Kohn-Rostoker coherent-potential-approximation calculations were performed to allow for a detailed and parameter-free discussion of the experimental data and their relationship to the electronic structure of the alloys.

I. INTRODUCTION

In contrast to the isoelectronic noble-metal systems Au-Cu and Ag-Au, the equilibrium phase diagram of the alloy system Ag-Cu (Ref. 1) exhibits simple eutectic behavior with a wide miscibility gap (Fig. 1). However, under certain nonequilibrium conditions the formation of a crystalline-disordered fcc alloy (γ phase) can be achieved. Duwez, Willens, and Klement[2] showed that by applying ultrafast quenching techniques to liquid Ag-Cu alloys, the segregation into the Ag- and Cu-rich phases α and β can be suppressed. The lattice constant of the resulting single-phased crystal varies smoothly with composition as is found by x-ray diffraction.[4–6] Until now few attempts were undertaken to investigate the electronic structure of such metastable alloys.[7–9] Here we present measurements of various physical properties related to the electronic structure, namely the linear coefficient of the low-temperature specific heat, the magnetic susceptibility, and the NMR Knight shift and spin-lattice relaxation time of ^{63}Cu in Ag-Cu. Moreover, charge-self-consistent Korringa-Kohn-Rostoker coherent-potential approximation (KKR-CPA) calculations were performed to allow for a detailed interpretation of experimental results. Because the alloy Ag-Cu is one of the most difficult systems to quench into the single-phased state,[10] we describe the sample preparation in some detail.

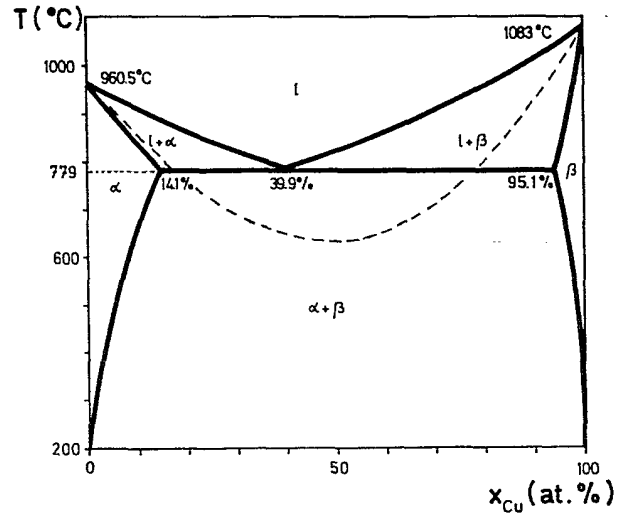

FIG. 1. Phase diagram of Ag-Cu (Ref. 1). The dashed line gives the minimum undercooling temperature T of liquid Ag-Cu necessary to obtain a transition to the metastable crystalline phase of the same composition (Ref. 43).

II. SAMPLE PREPARATION AND x-RAY ANALYSIS

The Ag-Cu alloys were prepared by Degussa (Hanau) by melting appropriate quantities of Ag (99.995%) and Cu (99.999%) and casting the liquid into crucibles. Samples with a nominal silver content of 10, 20, 30, 40, 50, 60, 70, 80, and 90 at. % were obtained this way. The various steps for this purpose were as follows: Pieces of approximately 0.5 g were cut off the alloy bars, cleaned in methanol, and etched in a H_2O_2/NH_4OH mixture for 30 s to remove surface contaminations. To prepare metastable single-phased samples from this starting material, we used a quenching apparatus that is based on the gun technique and is similar to that described by Davies and Hull.[11] The alloys were induction heated in a ceramic crucible under an argon atmosphere, melted, and held at a fixed temperature for 1 min. Then the liquid alloy was forced through a hole of 0.5-mm diameter in the crucible

by releasing a helium gas shock wave (pressure 7 MPa). The rapidly accelerated liquid alloy hit a water-cooled target and was quenched very quickly this way. Cooling rates of 10^6 K/s are normally achieved by means of this technique.[10,12] The resulting quenched alloy samples consisted of splats of different sizes. The material was separated into groups according to their size using meshes of different fineness. An x-ray diffractometer was used to determine the lattice constants of the splat material. Figure 2 shows the (111) reflex of $Ag_{50}Cu_{50}$ samples using Cu $K\alpha$ radiation. The cast but not quenched sample consists of two phases α and β, whereas the quenched alloy has formed the metastable γ phase and only two weak structures are left over from the α and β phases.

Many of the quenched alloy samples exhibited three lines of varying relative intensities originating from the α and β phases and the metastable γ phase, respectively. This was due to too slow cooling and therefore insufficient suppression of phase segregation. This problem has already been mentioned by Duwez.[10] To investigate this we define the phase segregation parameter S,

$$S=\frac{m_\gamma}{m_\alpha+m_\beta+m_\gamma}, \quad (1)$$

where m is the molar fraction of a specific case. The molar fraction was determined by measuring the intensities of the corresponding x-ray peaks and weighting them by the scattering powers of Cu and Ag. Obviously $S=0$ means total phase segregation and $S=1$ exclusive presence of the metastable phase. We found that S depends primarily on two parameters. First, on the size of the splats: the smaller they are the higher the value of S. This can easily be understood because the cooling rate for large particles on the cold target is much smaller than for small ones and therefore the suppression of the equilibrium phases α and β is less efficient. Second S depends on the initial temperature of the liquid metal before hitting the cooling target. Figure 3 shows S for the alloy $Ag_{60}Cu_{40}$ and three different splat sizes for various initial temperatures given as the temperature ΔT above the melting point (780 °C). Clearly the small particles have a greater content of the γ phase, as already mentioned. For the fine splats, however, a high initial temperature is necessary in order to suppress phase segregation. This stems from two effects. First, for too low initial temperatures the liquid metal cools down on its way to the target through the argon atmosphere, thus allowing partial or total crystallization (and subsequent segregation) before hitting the target. Second, even in the liquid alloy there might still be some local short-range order at temperatures only slightly above the melting point, therefore facilitating phase segregation after cooling down. For the large samples, however, a low initial temperature serves better to avoid phase segregation. This is because the hot drops take too much time to crystallize on the target when the initial temperature is too high. These considerations are completely consistent with the fact that a liquid-solid transition without a change in concentration occurs only if it is accompanied by a decrease of the Gibbs free enthalpy. From this thermodynamic require-

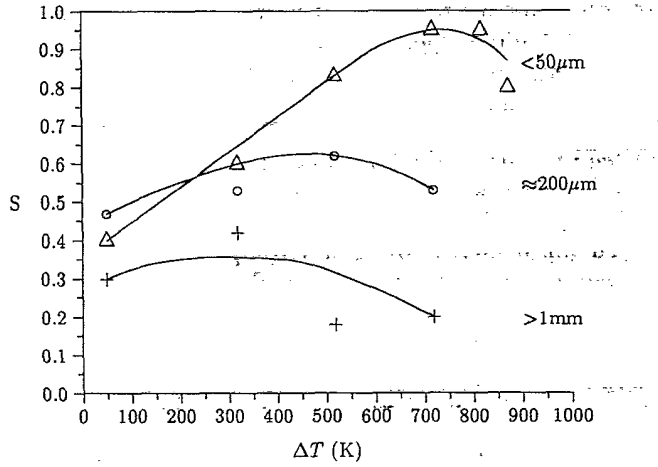

FIG. 3. Phase segregation parameter S for the alloy $Ag_{60}Cu_{40}$ and different splat diameters and temperatures ΔT above the melting point $T_m=780$ °C. Triangles: splat diameter <50 μm; circles: splat diameter ≈ 0.2 mm; crosses: splat diameter >1 mm.

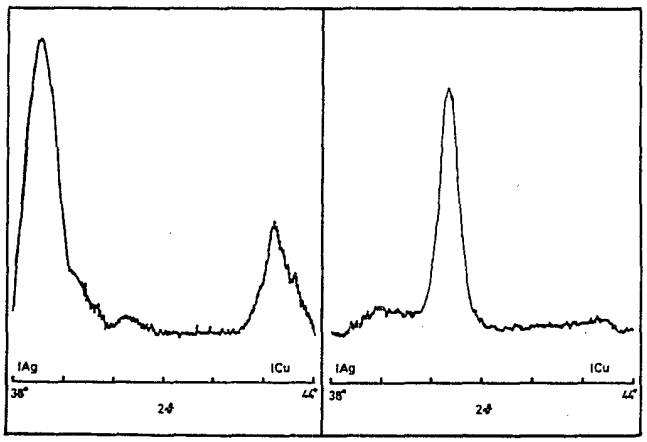

FIG. 2. X-ray diffractograms for $Ag_{50}Cu_{50}$ intensity vs diffraction angle 2θ. Left-hand side: powder (not quenched); right-hand side: quenched samples (splat diameter <50 μm). The positions of the pure metal diffraction peaks are marked.

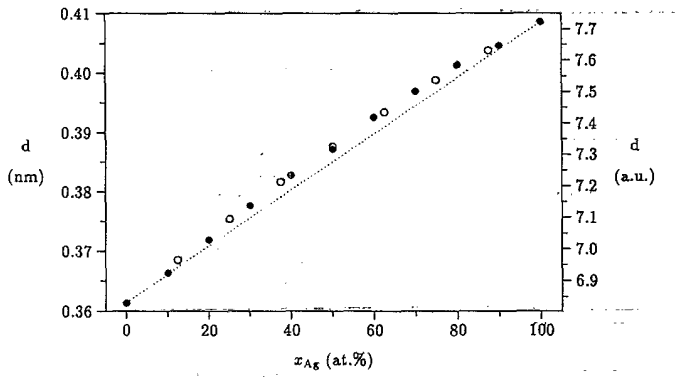

FIG. 4. Lattice constants of disordered single-phased metastable Ag-Cu alloys. Full circles: this work; open circles: Ref. 4. Dotted line: concentration-weighted mean lattice constant (Vegard line).

ment a minimum supercooling temperature T_0 can be derived that is included in Fig. 1.

Thus, the ideal conditions for the preparation of single-phase alloys are (a) to remove the large splats, and (b) to choose a sufficiently high but not too high initial temperature depending on the melting point of the alloy. For Ag-Cu and our apparatus we found $\Delta T \approx 500\,^{\circ}\mathrm{C}$ to be a good choice. For all available compositions of Ag-Cu approximately 0.5 g of single-phased splats ($S > 0.9$) were produced, requiring about 20 shots for each composition.

The measured lattice constants are shown in Fig. 4. These values vary smoothly with concentration and are in good agreement with the results of other authors.

III. SPECIFIC-HEAT MEASUREMENTS

The specific-heat measurements were performed by means of a quasiadiabatic method between 1.5 and 8 K. A newly developed apparatus used for the experiments operates automatically and has a temperature regulation based on a Cryocal germanium resistor.

Usually the low-temperature specific heat C of a metal or alloy is expressed in terms of a power series $C(T)=\gamma T+\beta T^3+\cdots$, where the first term stands for the electronic contribution and the second for the lattice contribution. While β is related to the Debye temperature Θ_D, γ is a direct measure for the total density of states $n(E_F)$ at the Fermi energy

$$\gamma=\tfrac{2}{3}\pi^2 k_B^2 n(E_F)(1+\lambda_{\mathrm{ep}}+\lambda_{\mathrm{sf}}+\cdots)\,, \tag{2}$$

where k_B is the Boltzmann constant. Compared to the bare density of states (DOS), electron-phonon coupling (λ_{ep}) and spin fluctuations (λ_{sf}), and probably other mechanisms in general, increase γ. A factor 2 occurs in Eq. (2) because we use the DOS per spin throughout the paper.

The accuracy of the raw data, plotted as C/T versus T^2 is better than 1% for our samples yielding an accuracy of about 1% for γ and 3% for Θ_D. The resulting values for γ are given in Fig. 5. They follow a fairly smooth function from Cu to Ag and connect the values for pure Ag and Cu taken from the literature by a nearly horizontal line.

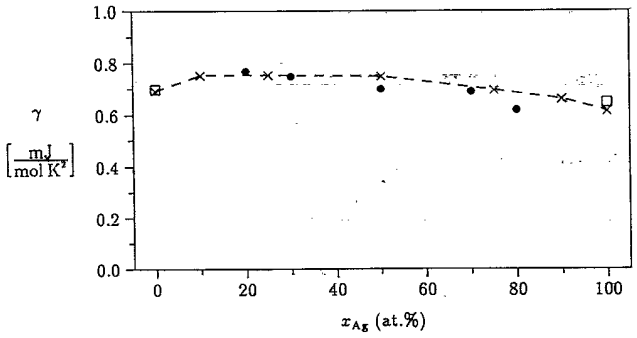

FIG. 5. Measured and calculated linear coefficient of the low-temperature specific heat γ of Ag-Cu. Full circles: γ measured in this work; squares: measurements by Ref. 13. Crosses: calculated γ (pure metal values by Ref. 14). For the calculation of γ from the DOS, Eq. (2) was used with a concentration-independent enhancement parameter $\lambda_{\mathrm{ep}}=0.05$.

IV. MAGNETIC-SUSCEPTIBILITY MEASUREMENTS

The magnetic susceptibility χ was measured by means of a Faraday balance where the force on the sample in an inhomogeneous magnetic field is used as a direct measure for the magnetic susceptibility. The maximum field which could be achieved by the apparatus was 0.8 T and the resolution of the balance was 10^{-9} N. An Oxford continuous flow cryostat allowed temperatures down to 4.2 K with a stability of 0.1 K. The apparatus was calibrated with $CoHg(SCN)_4$ which has a magnetic susceptibility of 16.45×10^{-6} emu/g at 300 K.[15] The field dependence of χ was determined at various temperatures and a Honda-Owen plot was used to eliminate the effects of ferromagnetic impurities. The resulting χ for the various temperatures were fitted numerically to the ansatz $\chi(T)=\chi(0)+C/T$, where the second term is a Curie-like contribution accounting for possible paramagnetic impurities.

The resulting $\chi(0)$, representing the susceptibility of the Ag-Cu matrix, is shown in Fig. 6. In our fitting procedure the small temperature dependence of the Ag-Cu samples that has to be expected from the properties of pure Ag and Cu (Refs. 16 and 17) has been ignored because for the investigated temperature range (4.2–300 K) it would be negligible compared to the error bars shown in Fig. 6. The measured susceptibilities are all negative and rather small. They are all very close to the

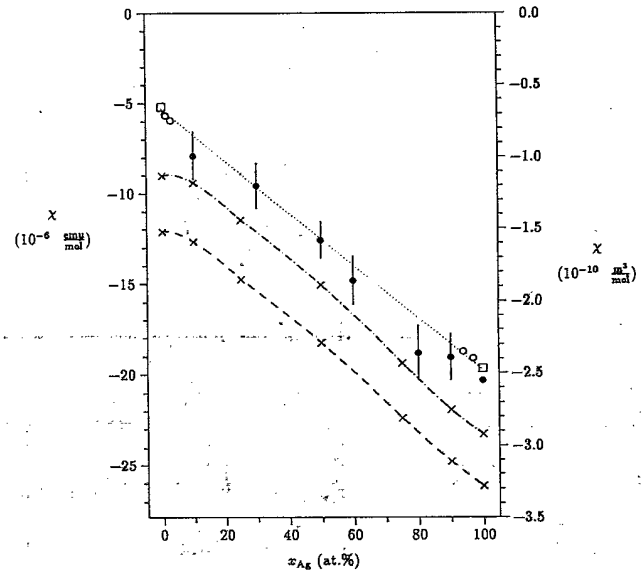

FIG. 6. Magnetic molar susceptibility of single-phased Ag-Cu at $T=4.2$ K. Full circles: this work; open circles: Ref. 18; squares: pure element values Refs. 16 and 17. The dotted line is the concentration-weighted mean experimental susceptibility. cgs units are shown on the left-hand side, SI units on the right. The crosses connected by the dash-dotted line give the sum of the theoretical Pauli spin susceptibility and the diamagnetic susceptibility, $\chi_p+\chi_{\mathrm{dia}}$. An estimate for $\chi_p+\chi_{\mathrm{dia}}+\chi_L$ is represented by the crosses on the dashed line.

concentration-weighted mean susceptibility (dashed line). Literature values of χ for small Ag and Cu concentrations[18] fit well into the measured overall tendency.

V. NMR MEASUREMENTS

A modified Bruker pulsed NMR spectrometer [soft x-ray photoemission (SXP)] was used for measuring the spin-lattice relaxation time T_1 and Knight shift K of ^{63}Cu in Ag-Cu alloys. An Oxford Cryomagnet was operated at 5 T corresponding to a resonance frequency of about 55 MHz. The cryostat allowed cooling down to 4.2 K. At this temperature all measurements were done.

For the measurement of the *spin-lattice relaxation time* 15 $\pi/2$ (20 μs) saturation pulses were applied in order to destroy the longitudinal magnetization in the sample. After a delay time τ the recovered magnetization was monitored by a sequence of two $\pi/2$ pulses. The intensity of the resulting spin echo, determined by integration, was assumed to be proportional to the longitudinal magnetization $M_z(\tau)$. In order to determine the relaxation time T_1 we measured $M_z(\tau)$ for 40–50 delay times τ and fitted a biexponential function to the data by a least-square procedure

$$M_z(\tau)=M_0+(M_\infty-M_0)(1-\tfrac{2}{5}e^{-\tau/T_1}-\tfrac{3}{5}e^{-6(\tau/T_1)}) . \tag{3}$$

This function describes the recovery of the nuclear magnetization for a nuclear spin $I=\frac{3}{2}$ after saturation of the central transition.[19] In Eq. (3) M_0 is the rest magnetization not removed by the saturation pulses, M_∞ the equilibrium magnetization. The spin-lattice relaxation time could be determined only for the copper-rich alloys with sufficient accuracy while for the silver-rich alloys the data could not be fitted to the function in Eq. (3) properly. The resulting spin-lattice relaxation rate $(T_1T)^{-1}$ for the copper-rich samples is shown in Fig. 7, exhibiting a slight, nearly linear increase with increasing silver content. The two values on the copper-rich side by Fromhold[20] are compatible with our measurements whereas

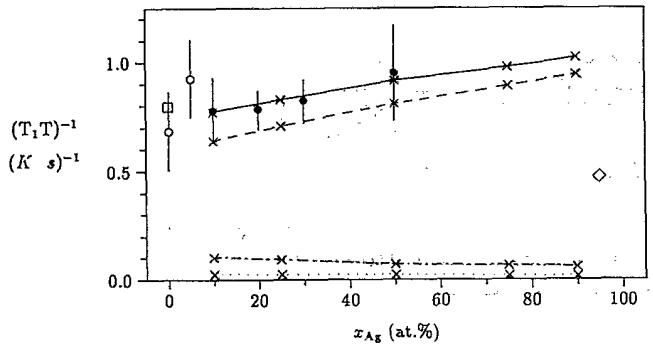

FIG. 7. Nuclear spin-lattice relaxation rate $(T_1T)^{-1}$ of ^{63}Cu in single-phased Ag-Cu. $T=4.2$ K, $B_0=5$ T, $\nu\approx55$ MHz. Full circles: this work; open circles: Ref. 20; diamond: Ref. 21; square: Ref. 22. The theoretical rate is represented by crosses connected by a full line. Its decomposition into s, p, and d contributions according to Eq. (8) are marked by crosses on a dashed, dotted, or dash-dotted line, respectively.

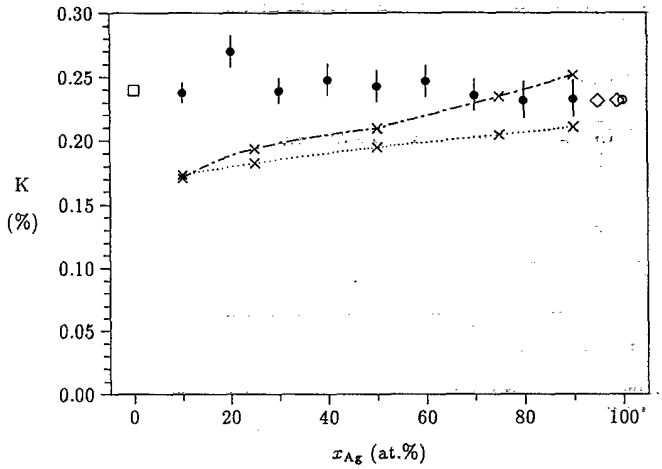

FIG. 8. Knight shift of ^{63}Cu in single-phased Ag-Cu. $T=4.2$ K, $B_0=5$ T, $\nu\approx55$ MHz. Full circles: this work; diamond: Ref. 21; open circle: Ref. 23; square: Ref. 22. The crosses on the dotted line give the direct contribution K_{fc}^{dir} to the Knight shift according to Eq. (10), while the crosses on the dash-dotted line represent K_{fc} according to Eq. (11).

the value by Matzkanin *et al.*[21] for 95% Ag is much higher than we would expect from extrapolating our measurements or from our calculations (see the next section). We assume that the influence of quadrupolar interaction on the nuclear recovery behavior expressed by Eq. (3) has not been taken into account by these authors.

The *Knight shifts* were obtained from spin-echo profiles by varying the field continuously over a range of about 20 mT around the resonance position while the spin echo produced by applying two $\pi/2$ pulses was observed. In Fig. 8 the resulting shifts are shown. These data are based on the nuclear gyromagnetic ratio $\gamma/2\pi=11.285$ MHz/T for ^{63}Cu, corresponding to a Knight shift of 0.238% for pure copper.[22,24] Except for 20% Ag all values follow a smooth line from Cu to Ag. The values of two other authors for the diluted range[21,23] and the pure metal[22] support our results.

VI. ELECTRONIC STRUCTURE CALCULATIONS

As is obvious from the equilibrium phase diagram of Ag-Cu in Fig. 1, the components of this system show only very limited solubility in the solid phase. This behavior could be explained by Robbins and Falicov[25] on the basis of electronic structure calculations using a tight-binding-like Hamiltonian. More recently Sanchez, Stark, and Moruzzi[26] were able to calculate the miscibility gap of the solid phase using the cluster variational method (CVM) proposed by Kikuchi.[27] Following the suggestion of Conolly and Williams,[28] the effective multisite interaction parameters entering these calculations could be derived from first-principles band-structure calculations for hypothetical ordered Ag-Cu alloys. In contrast to this situation an adequate description of the electronic properties of our metastable single-phased samples requires treatment of these systems as random alloys. Such treatment can be achieved in a very rigorous way by applying the Korringa-Kohn-Rostoker (KKR)

method of band-structure calculations in connection with the coherent-potential-approximation (CPA) alloy theory.[29,30]

We used this KKR-CPA method to calculate the electronic structure of a number of Ag-Cu alloys in a self-consistent manner within the framework of the local-density-functional theory. The resulting DOS curves for three different compositions are shown in Fig. 9. Obviously these curves exhibit a pronounced split-band behavior. For all compositions the Ag and Cu d-band complexes are energetically well separated from each other. While the Cu-related structure is centered at around 2 eV below the Fermi energy, that of Ag lies about 6 eV below the Fermi level. In $Ag_{10}Cu_{90}$ and $Ag_{90}Cu_{10}$ the majority component contributes to the DOS with a broad peaky structure very similar to the pure metal. The minority component, however, shows a bell-shaped DOS characteristic for a virtual bound state. For all compositions the Fermi energies lie well above the Cu-related d-band complex in a region where the DOS varies only slowly with energy. All these findings are in full accordance with the ultraviolet photoemission spectroscopy (UPS) data of Shevchik and Goldmann[8] as well as with the interpretation of the optical investigations of Nielsson and Forssell[7] and Rivory[9] on evaporated polycrystalline films.

In contrast to these experimental investigations, the measurements presented in this paper are intimately related to the electronic properties at the Fermi energy. For this reason we give the angular-momentum-resolved partial DOS at this energy in Table I. As one can see for both components, these quantities show a similar variation with concentration, namely an increase with Ag content. This behavior can at least partially be related to the accompanying increase of the lattice constant (Fig. 4). The most striking difference between the data for Ag and Cu occurs for the d-like DOS which is more than twice as large for Cu as for Ag. Clearly this reflects the fact that the d-band complex of Ag lies at a much higher binding energy than that of Cu, as can be seen in Fig. 9.

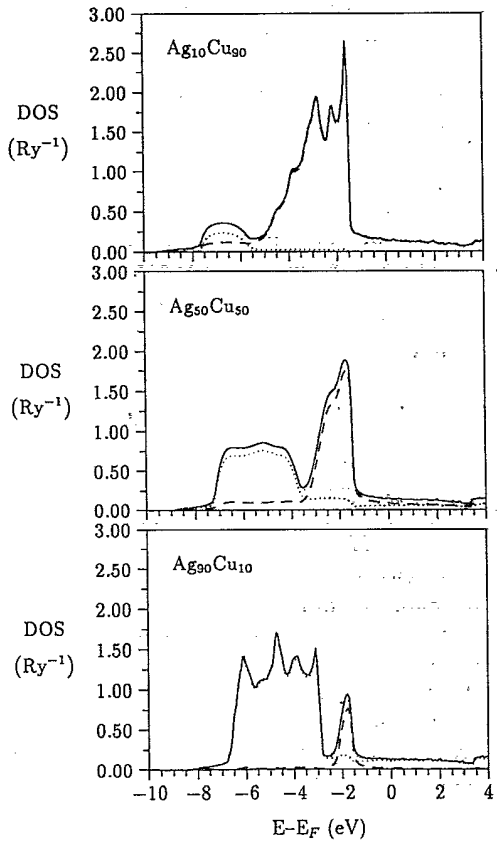

FIG. 9. Total densities of states for disordered Ag-Cu alloys (full line). Concentration-weighted local DOS for Ag (dotted line) and Cu (dashed line) are also shown. The energy is given with respect to the Fermi energy.

TABLE I. Angular-momentum-resolved partial DOS at the Fermi energy of Ag and Cu in disordered Ag-Cu and corresponding total DOS. The values for the pure components were taken from Ref. 14. All values are given in units of states/Ry spin atom.

x_{Ag}	$n_s^{Cu}(E_F)$	$n_p^{Cu}(E_F)$	$n_d^{Cu}(E_F)$	$n_s^{Ag}(E_F)$	$n_p^{Ag}(E_F)$	$n_d^{Ag}(E_F)$	$n(E_F)$
0	0.271	0.744	0.980				2.00
10	0.291	0.726	1.126	0.244	0.680	0.510	2.07
25	0.322	0.766	1.168	0.269	0.725	0.535	2.07
50	0.368	0.846	1.230	0.307	0.807	0.561	2.06
75	0.409	0.854	1.243	0.331	0.823	0.563	1.91
90	0.433	0.883	1.251	0.315	0.855	0.566	1.82
100				0.358	0.939	0.480	1.78

In the next section we shall use the data summarized in Table I together with some additional quantities derived from our electronic structure calculations, to give a detailed interpretation of the experimental material presented above.

VII. DISCUSSION

A. Low-temperature specific-heat coefficient γ

For multicomponent systems the low-temperature specific-heat coefficient γ supplies a rather direct probe of the total DOS at the Fermi energy. For the alloy system studied here, the enhancement of γ due to spin fluctuations in comparison to the bare value [see Eq. (2)] can be ignored. For the pure components the electron-phonon enhancement factor λ_{ep} has been calculated by various authors using the so-called rigid muffin-tin approximation due to Gaspary and Gyorffy.[31] This approach has been generalized to be applicable to random alloys by Gyorffy, Pindor, and Temmerman,[32] leading to an expression containing local averages of the mean-square displacement of the corresponding atom which for pure systems may be estimated using the Debye temperature[33] and containing the so-called Hopfield parameter. This parameter is a purely electronic quantity and is determined by the angular-momentum-resolved partial DOS, the corresponding phase shifts, and the Fermi energy. Because λ_{ep} has substantial contributions related to the f states[33] and our calculations were restricted to $l_{max}=2$, i.e., d electrons, we could not use the expressions given by Ref. 32 to evaluate λ_{ep} for the Ag-Cu system. Fortunately it turns out that λ_{ep} for pure Cu and for pure Ag are quite small and similar to each other. Papaconstanto-

poulos *et al.*[33] find $\lambda_{ep}^{Cu}=0.069(0.058)$ and $\lambda_{ep}^{Ag}=0.059(0.051)$, where the values given in parentheses were obtained by reducing the *d-f* contribution to λ_{ep} by half to account for some shortcomings of the rigid muffin-tin model. Thus, it seems reasonable to assume λ_{ep} lies between 0.05 and 0.06 throughout the entire concentration range. Using Eq. (2) we therefore set λ_{ep} to 0.05 to calculate γ. As can be seen in Fig. 5 both sets of data indicate a slight maximum on the Cu-rich side of the system, and the resulting theoretical γ is therefore in very satisfying agreement with the experimental results.

B. Magnetic susceptibility

As for the low-temperature specific-heat coefficient γ, the magnetic susceptibility is intimately connected with the electronic structure at the Fermi energy. Similar to Eq. (2) the Pauli contribution χ_p to χ can be written as (cgs units)

$$\chi_p=2\mu_B n(E_F)S \ . \tag{4}$$

Here the Stoner enhancement factor S accounts for the influence of exchange and correlation. Within the framework of spin-density functional theory S can be obtained from the expression

$$S=\frac{1}{1-In(E_F)} \ , \tag{5}$$

with I the Stoner parameter or integral.[34] For pure Cu as well as for pure Ag S has been found to be 1.12 by Janak.[34] Although Eq. (5) is strictly applicable in this form only to pure systems, there is no reason to expect any remarkable deviation of S from this value for the Ag-Cu system. This could indeed be verified by performing self-consistent spin-polarized calculations taking an external field of several mRy into account. The spin susceptibility determined from the induced spin moment and the external field agreed in all cases within some few percent with the susceptibility obtained from Eq. (4) using the concentration-dependent DOS and $S=1.12$. Thus, χ_p follows the variation of $n(E_F)$ as given in Table I.

In addition to the spin there is an orbital contribution to the susceptibility, which can be further split into the diamagnetic, the Landau, and the Van Vleck susceptibility[35]

$$\chi_{orb}=\chi_{dia}+\chi_L+\chi_{VV} \ . \tag{6}$$

The diamagnetic term is proportional to the expectation value of r^2 evaluated within the Wigner-Seitz cell and summed for all the electrons within that region. For most of the pure elements with $Z\leq 48$, χ_{dia} has been given in a previous publication by Banhart *et al.*[36] As it has been shown by these authors, it is a very good approximation to replace χ_{dia} for an alloy by the sum of the concentration-weighted diamagnetic susceptibilities of the pure constituents. Using χ_{dia} for Cu and Ag, -19.4 and -33.0×10^{-6} emu/mol, respectively, we give in Fig. 6 the sum of the spin and diamagnetic susceptibility. Obviously the variation of χ with the concentration is dominated by the diamagnetic contribution.

Comparing $\chi_p+\chi_{dia}$ to the experimental data one has to conclude that there is an appreciable contribution to the total susceptibility due to χ_L and χ_{VV} of around 3×10^{-6} emu/mol. This conclusion is supported by the theoretical results of Yasui, Takahashi, and Callaway[37] for the total orbital susceptibility χ_{orb} of pure Cu and Ag: -10 and -35×10^{-6} emu/mol, respectively. Unfortunately the approach of Yasui, Takahashi, and Callaway does not allow for splitting the orbital susceptibility according to Eq. (6) in a straightforward way. Subtracting the values for χ_{dia} given above, one finds $\chi_L+\chi_{VV}$ to be $+9.4$ and -2×10^{-6} emu/mol for Cu and Ag, respectively. Although the value for pure copper is obviously too high, as can be seen by adding χ_p to Yasui's χ_{orb} and comparing it with the experimental data in Fig. 6, these figures give the correct order of magnitude for $\chi_L+\chi_{VV}$ expected from Fig. 6. To get an estimate for the Van Vleck contribution on the basis of the available data, one may approximate χ_L by[38]

$$\chi_L=-\frac{1}{3}\left[\frac{m}{m^*}\right]^2\chi_p^0 \ . \tag{7}$$

Here m (m^*) is the (effective) electronic mass and χ_p^0 the nonenhanced Pauli susceptibility, i.e., χ in Eq. (4) without the factor S. This relation was derived for nearly free-electron systems and may serve as a crude estimate of χ_L for the present case by setting $m=m^*$. Adding the corresponding term to $\chi_p+\chi_{dia}$ gives the dashed line in Fig. 6. The distance of this curve from the experimental data has to be ascribed to χ_{VV} which is obviously quite high and of the same order of magnitude as χ_p.

Although this analysis clearly demonstrates the importance of χ_{VV} for Ag-Cu it should be emphasized that, primarily because of the use of Eq. (7), reliable quantitative data for χ_{VV} can only be obtained by a corresponding direct calculation of this term.[32]

C. Nuclear spin-lattice relaxation rate $(T_1T)^{-1}$ of ^{63}Cu

In contrast to the specific-heat coefficient γ and the magnetic susceptibility χ the nuclear spin-lattice relaxation rate $(T_1T)^{-1}$ supplies a very distinct and component-specific probe for the electronic properties at the Fermi energy. This appealing property is evident from the following expressions for the rate $(T_1T)_\alpha^{-1}$ of the component α:[39]

$$(T_1T)_\alpha^{-1}=\sum_i (T_1T)_{\alpha,i}^{-1} \ , \tag{8}$$

$$(T_1T)_{\alpha,i}^{-1}=\sum_l C_{i,l}^\alpha[\gamma_n^\alpha B_{i,l}^\alpha n_l^\alpha(E_F)]^2 \ . \tag{9}$$

Here l is the angular-momentum quantum number and the index i stands for the various coupling mechanisms between the nuclear and electronic systems, i.e., the Fermi contact, the dipolar, and the orbital hyperfine interaction. γ_n^α is the nuclear gyromagnetic ratio, the $C_{i,l}^\alpha$ contain some constants and express the selection rules, and the $B_{i,l}^\alpha$, finally, are the so-called hyperfine fields. Explicit

expressions for the $C^{\alpha}_{i,l}$ and $B^{\alpha}_{i,l}$ are given in Ref. 39, e.g., and a derivation of the corresponding formulas can be found in references given therein. Within a nonrelativistic description of the electronic structure the hyperfine field connected with the Fermi contact interaction is proportional to the electronic density at the nuclear region and therefore is nonzero only for s electrons. The dipolar and orbital hyperfine fields, on the other hand, occur only for p and d electrons. Both fields for a given angular momentum l are identical and represent the expectation value of r^{-3} for the corresponding partial-wave function.

Because relativistic effects may influence the hyperfine interaction even for relatively light elements,[39] we used a scalar-relativistic description of the electronic structure to account for the mass enhancement and the Darwin correction. This approach, however, demands the use of modified expressions for the hyperfine fields, which have been derived by Blügel *et al.*[40]

Results for $(T_1T)^{-1}_{\mathrm{Cu}}$ based on Eq. (8) are shown in Fig. 7. Obviously the agreement with experiments is very satisfying. Because the experimental data point at 95 at. % Ag neither fits our theoretical nor the other experimental data it is assumed that it is erroneous, presumably because the authors did not take into account the influence of quadrupolar interaction as we did using Eq. (3).

The angular-momentum decomposition of $(T_1T)^{-1}_{\mathrm{Cu}}$ also given in Fig. 7 shows that it is dominated by its s contribution. For the non-s electrons the orbital part is much more important than the dipolar contribution. The ratio of the orbital to the dipolar part is 10:3 for p electrons and 14:1 for d electrons, assuming a relative weight of the t_{2g}- to the e_g-like states of 3:2.[39]

As can be seen from Fig. 7, the d contribution exceeds the p part for all concentrations because of the higher related DOS $n^{\mathrm{Cu}}_{\alpha}(E_F)$, although the corresponding hyperfine fields are somewhat smaller. Moreover $(T_1T)^{-1}_{\mathrm{Cu},p}$ and $(T_1T)^{-1}_{\mathrm{Cu},d}$ do not increase with Ag concentration, although one would expect that from the concentration dependence of $n^{\mathrm{Cu}}_{p}(E_F)$ and $n^{\mathrm{Cu}}_{d}(E_F)$. This is due to the decrease in the hyperfine field which is caused by a reduction of $\langle r^{-3}\rangle$ due to the lattice expansion with increasing Ag content. This also affects the other hyperfine fields but does not compensate for the increase in $n^{\mathrm{Cu}}_{s}(E_F)$ for the Fermi contact part of $(T_1T)^{-1}_{\mathrm{Cu},s}$. This finally leads to the observed increase of the total rate with increasing Ag concentration.

D. Knight shift of ^{63}Cu

Analogous to the susceptibility χ the Knight shift K is of spin and orbital origin. For cubic systems the spin part stems exclusively from s electrons via the Fermi contact interaction. If one assumes that this contribution to the Knight shift is only due to the imbalance of the s electrons of spin up or down, induced by the external magnetic field, it may be expressed as

$$K^{\mathrm{dir}}_{\mathrm{fc}} = SB_s\mu_B n_s(E_F) \ . \tag{10}$$

Here B_s is just the hyperfine field produced by one S electron and is identical to that entering Eq. (8). Figure 8 gives the direct contribution $K^{\mathrm{dir}}_{\mathrm{fc}}$ to the Knight shift of ^{63}Cu in Ag-Cu calculated according to Eq. (10) by a dotted line. As for $(T_1T)^{-1}$ this term increases monotoneously with the Ag concentration. This behavior is more pronounced for $K^{\mathrm{dir}}_{\mathrm{fc}}$ than for $(T_1T)^{-1}$ because here only the increasing s part is present while for $(T_1T)^{-1}$ it is partially compensated for by the decreasing d part. Comparison with the experimental shifts in Fig. 8 shows that $K^{\mathrm{dir}}_{\mathrm{fc}}$ alone already accounts for most of the shifts.

Although Eq. (10) accounts for the Stoner enhancement via the factor S it completely neglects any contribution to K due to a distortion of the wave functions by the induced charges in the exchange-correlation potential. A straightforward way of accounting for this polarization mechanism is to perform spin-polarized electronic structure calculations including an external field. In this case the Fermi contact Knight shift is given by (cgs units)

$$K_{\mathrm{fc}} = \frac{8\pi}{3}\frac{m(0)}{B_{\mathrm{ext}}} \ , \tag{11}$$

where $m(0)$ is the spin magnetization induced at the nuclear site by an external field of strength B_{ext}. As for the hyperfine fields this expression has to be used in a modified form if a scalar-relativistic description of the electronic structure has been adopted, as was done here.[40]

In Fig. 8 results obtained using Eq. (11) are represented by a dash-dotted line. The contribution to these shifts from the polarization of the core wave functions turned out to increase only very slightly in the magnitude from -0.015% to -0.017% from the Cu-rich to the Ag-rich side of the system. This variation is completely compatible with the experience that this contribution to K is proportional to the local spin susceptibility.[41] Because the core polarization contribution is rather small in magnitude one can ascribe the difference of the direct and total Fermi contact Knight shift to the polarization of the conduction-band electrons. Here one should note that the division of K_{fc} according to Eq. (11) into core and conduction-band polarization and the direct contribution is not always sensible. For systems where the Stoner enhancement of the pure constituents is very different, pronounced intersite effects may occur which may even give rise to a negative shift, as for example for Ag in Pd-rich Ag-Pd.[42] However, this does definitely not apply to Ag-Cu.

Comparing the total Fermi contact shift K_{fc} to the experimental data points K_{exp} in Fig. 8, one realizes that the agreement has improved compared with that using $K^{\mathrm{dir}}_{\mathrm{fc}}$ instead of K_{fc}. Nevertheless, there is still some discrepancy left. Apart from the problem of choosing a suitable diamagnetic standard to which the experimental Knight shift is referred, the only explanation for this is a contribution due to the orbital Van Vleck term.[41] This conclusion seems plausible in light of the discussion of the susceptibility given above. Unfortunately neither the Van Vleck susceptibility nor the closely related Van Vleck Knight shift K_{VV} is related to the electronic structure in a simple way. In fact K_{VV} has been calculated only for very few systems (V, Cr, Nb, Mo: Ref. 41; Li, Na, K, $YBa_2Cu_3O_7$: Ref. 43). Although the spatial and electronic structure of $YBa_2Cu_3O_7$ has no direct relation-

ship to that of the system studied here, it should be noted that in this case noticeable orbital contributions to the Cu Knight shift have been found.

VIII. SUMMARY

(i) Single-phased metastable Ag-Cu alloys could be produced for the whole composition range applying ultrafast quenching techniques and by optimizing the process parameters.

(ii) The measured values of the linear coefficient of the low-temperature specific heat, the ^{63}Cu spin-lattice relaxation rate, and the ^{63}Cu Knight shift are found to be only weakly concentration dependent, whereas the magnetic susceptibility exhibits a nearly constant slope when seen as a concentration-dependent function.

(iii) The densities of states, specific-heat coefficients, susceptibilities, spin-lattice relaxation rates, and Knight shifts calculated by means of the fully self-consistent KKR-CPA method allow for a satisfactory explanation of the experimental findings.

ACKNOWLEDGMENT

We would like to thank Degussa (Hanau) for supplying Ag-Cu alloy samples.

*Deceased.

[1]M. Hansen and K. Anderko, *Constitution of Binary Alloys* (McGraw-Hill, New York, 1958).

[2]P. Duwez, R. H. Willens, and W. Klement, J. Appl. Phys. **31**, 1136 (1960).

[3]T. B. Massalski and Y. Bienvenue, in *Rapidly Quenched Metals*, edited by N. J. Grant and B. C. Giessen (MIT Press, Cambridge, 1975), p. 95.

[4]W. Klement, Ph.D thesis, CIT, Pasadena (1962).

[5]R. K. Linde, J. Appl. Phys. **37**, 934 (1966).

[6]S. Nagakura, S. Toyama, and S. Oketani, Acta Metall. **14**, 73 (1966).

[7]P. O. Nielsson and G. Forsell, J. Phys. (Paris) Colloq. **34**, C4-57 (1974).

[8]N. J. Shevchik and A. Goldmann, J. Electron Spectrosc. Relat. Phenom. **5**, 631 (1974).

[9]J. Rivory, Phys. Rev. B **15**, 3119 (1977).

[10]P. Duwez, Prog. Solid State Chem. **3**, 377 (1966).

[11]H. A. Davies and J. B. Hull, J. Mater. Sci. **9**, 707 (1974).

[12]R. C. Ruhl, Mater. Sci. Eng. **1**, 313 (1967).

[13]D. L. Martin, Phys. Rev. B **8**, 5357 (1973).

[14]T. Asada, K. Terakura, and T. Jarlborg, J. Phys. F **11**, 1847 (1981).

[15]H. S. Räde, J. Phys. Chem. **77**, 424 (1973).

[16]R. Bowers, Phys. Rev. **102**, 1486 (1956).

[17]C. M. Hurd, J. Phys. Chem. Solids **27**, 1371 (1966).

[18]W. G. Henry and J. L. Rogers, Can. J. Phys. **38**, 908 (1960).

[19]E. R. Andrew and D. P. Tunstall, Proc. Phys. Soc. **78**, 1 (1961).

[20]A. T. Fromhold, J. Chem. Phys. **52**, 2871 (1970).

[21]G. A. Matzkanin, J. J. Spokas, C. K. Sowers, and D. O. vanOstenburg, Phys. Rev. **181**, 559 (1969).

[22]U. El-Hanany and D. Zamir, Phys. Rev. B **5**, 30 (1972).

[23]T. J. Rowland and F. Borsa, Phys. Rev. **134A**, 743 (1964).

[24]G. C. Carter, L. H. Bennett, and D. J. Kahan, Prog. Mater. Sci. **20**, 153 (1977).

[25]M. O. Robbins and L. M. Falicov, Phys. Rev. B **25**, 2343 (1982).

[26]J. M. Sanchez, J. P. Stark, and V. L. Moruzzi, Phys. Rev. B **44**, 5411 (1991).

[27]R. Kikuchi, Phys. Rev. **81**, 988 (1951).

[28]J. W. Conolly and A. R. Williams, Phys. Rev. **27**, 5169 (1983).

[29]H. Winter and G. M. Stocks, Phys. Rev. B **27**, 882 (1983).

[30]H. Akai, J. Phys. Condens. Matter **1**, 8045 (1989).

[31]G. D. Gaspary and B. L. Gyorffy, Phys. Rev. Lett. **28**, 801 (1972).

[32]B. L. Gyorffy, A. Pindor, and W. M. Temmerman, Phys. Rev. Lett. **43**, 1343 (1979).

[33]D. A. Papaconstantopoulos, L. L. Boyers, B. M. Klein, A. R. Williams, V. L. Moruzzi, and J. F. Janak, Phys. Rev. B **15**, 4221 (1977).

[34]J. F. Janak, Phys. Rev. B **16**, 255 (1977).

[35]J. Benkowitsch and H. Winter, J. Phys. F **13**, 991 (1983).

[36]J. Banhart, H. Ebert, J. Voitländer, and H. Winter, J. Magn. Magn. Mater. **61**, 221 (1986).

[37]M. Yasui, T. Takahashi, and J. Callaway, J. Phys. Condens. Matter **3**, 2679 (1991).

[38]R. M. White, *Quantum Theory of Magnetism* (McGraw-Hill, New York, 1970).

[39]H. Ebert, H. Winter, and J. Voitländer, J. Phys. F **14**, 2433 (1984).

[40]S. Blügel, H. Akai, R. Zeller, and P. H. Dederichs, Phys. Rev. B **35**, 3271 (1987).

[41]H. Ebert, H. Winter, and J. Voitländer, J. Phys. F **16**, 1133 (1986).

[42]H. Ebert and H. Winter, Solid State Commun. **63**, 899 (1987).

[43]W. Götz and H. Winter (unpublished).